Speckle Imaging: a boon for astronomical observations

S. K. Saha
Indian Institute of Astrophysics
Bangalore - 560 034
e-mail: sks@iiap.ernet.in

Abstract

The speckle imaging is a photographic technique that resolves objects viewed through severely distorted media. The results are insensitive to the errors caused by apparent size of the isoplanatic patch and the telescope aberrations. In this article, a short descriptions of the atmospheric turbulence and its effect on the flat wavefront from a stellar source is presented; the shortcomings of the conventional long-exposure images in the presence of Earth's atmosphere are discussed. The advantages of the speckle interferometric technique over conventional imaging are enumerated. The technical details of the method, basic Fourier optics, data analysis procedures are also described.

1. Introduction

The atmosphere of earth restricts the resolution of conventional ground based astronomical images to about 1 arc second. This is due to the refractive index variations of the atmosphere through which the light rays reaching the telescope. When a star image is observed through a telescope with high magnification, the observed image structure is usually far from the theoretical pattern. The appearance of image depends strongly on the size of aperture of the telescope. Large telescope helps in gathering more optical energy, as well as in obtaining better angular resolution. The resolution increases with the diameter of the aperture. For example, the diffraction-limit of a 2.34 meter telescope is about 0.05 arc second. But in reality, the image is degraded by factor of 20. With small aperture a random motion of a image is often affect the main effect, whereas, with large aperture spreading and blurring of the image occur.

Owing to the diffraction phenomenon, the image of the point source (unresolved stars) cannot be smaller than a limit at the focal plane of the telescope. This phenomenon can be observed in ocean, when regular waves pass through an aperture. It is present in the sound waves, as well as in the electro-magnetic spectrum too starting from gamma rays to radio waves.

Speckle interferometric technique (Labeyrie, 1970) yields the diffraction-limited autocorrelation of the object. The diffraction-limited resolution of celestial objects viewed through the Earth's turbulent atmosphere could be achieved with the largest optical telescope, by post detection processing of a large data set of short-exposure images using Fourier-domain methods. Certain specialized moments of the Fourier transform of a short-exposure image contain diffraction-limited information about the object of interest. In this article, I shall describe a few basic theorems of Fourier optics, which are essential to understand this technique followed by the theory of speckle interferometry. The data processing method to analyze specklegrams of close binary stars obtained with 2.34 meter Vainu Bappu telescope (VBT), Kavalur, India is also discussed.

2. Preamble

In order to obtain high angular resolution of an stellar object, Fizeau (1868) had suggested to install a screen with two holes on top of the telescope that produce Young's fringes at its focal plane as the fringes remain visible in presence of seeing, thus allowing measurements of stellar diameters. Stefan attempted with 1 meter telescope at Observatoire de Marseille but could not notice any significant drop of fringe visibility and opined none of the observed stars approached 0.1 arc-seconds in angular size. About half a century later, Michelson could measure the diameter of the satellites of Jupiter with Fizeau interferometer on top of the Yerkes refractor. With the 100 inch telescope at Mt. Wilson (Anderson, 1920), the angular separation of spectroscopic binary star Capella was measured.

To overcome the restrictions of the baseline, Michelson (1920) constructed the stellar interferometer equipped with 4 flat mirrors to fold the beams by installing a 7 meter steel beam on top of the afore-mentioned 100 inch telescope; the supergiant star α Orionis were resolved (Michelson and Pease, 1921). Due to the various difficulties, viz., (i) effect of atmospheric turbulence, (ii) variations of refractive index above small sub-apertures of the interferometer, and (iii) mechanical instability, the project was abandoned.

The field of optical interferometry lay dormant until it was revitalized by the development of intensity interferometry (Brown and Twiss, 1958). Success in completing the intensity interferometer at radio wavelengths (Brown et al., 1952), in which the signals at the antennae are detected separately and the angular diameter of the source is obtained by measuring correlation of the intensity fluctuations of the signals as a function of antenna separation, Brown and Twiss (1958) demonstrated its potential at optical wavelengths by measuring the angular diameter of Sirius. Subsequent development of this interferometer with a pair of 6.5 meter light collector on a circular railway track spanning 188 meter

(Brown et al., 1967), depicted the measurements of 32 southern binary stars with angular resolution limit of 0.5 milliarcseonds (Brown, 1974). The project was abandoned due to lack of photons beyond 2.5 magnitude stars.

Meanwhile, Labeyrie (1975) had developed a long baseline interferometer − Interfèromētre *à* deux telescope (I2T) − using a pair of 25 cm telescopes at Observatoire de Calern, France. His design combines features of the Michelson and of the radio interferometers. The use of independent telescopes increases the resolving capabilities. In this case, coude beams from both the telescopes arrive at central station and recombines them. This interferometer obtained the first measurements for a number of giant stars (Labeyrie, 1985). Following the success of its operation, he undertook a project of building large interferometer known as grand interfèromētre *à* deux telescope (GI2T) at the same observatory. This interferometer comprises of two 1.5 meter spherical telescopes on a North-South baseline, which are movable on a railway track (Labeyrie et al., 1986). Mourard et al. (1989) had resolved the rotating envelope of hot star γ Cassiopeiae using this interferometer. The technical details of this kind of interferometers can be found in the recent article by Saha (1999a).

There are several long baseline interferometers that are in operation; some are at various stages of development (Saha, 1999a). These interferometers are based on the principle of merging speckles from both the telescopes. In other words, the fringed speckle can be visualized when a speckle from one telescope is merged with the speckle from the other telescope. Therefore, it is necessary to get acquainted with relatively new topics, speckle interferometry. In what follows, the formation of speckles and the way to decode the atmospherically degraded informations are discussed in brief.

3. Convolution and its applications

The convolution of two functions is a mathematical procedure (Goodman, 1968) which simulates phenomena such as a blurring of a photograph. That may be caused by poor focus, by the motion of a photographer during the exposure, by dirt on the lens etc. In such blurred picture each point of object is replaced by a spread function. The spread function is disk shaped in the case of poor focus, line shaped if the photograph has moved, halo shaped if there is a dust on lens. In other words, we know that delta function has value at a single point otherwise it is zero. But generally the measurement does not produce this.

Let us consider an input curve that can be represented by the curve $f(x)$ in terms of lot of close delta functions which are spread. Here, the shape of the response of the system including unwanted spread, is same for all values of x (invariant for each considered delta function). Now, the value of the function

$f(x)$ at x_1 is $f(x') \star g(x_1 - x')$. This is similar for each considered point on the curve. So for the whole curve, we define mathematically

$$h(x) = \int_{-\infty}^{+\infty} f(x')g(x - x')dx', \tag{1}$$

where, $h(x)$ is the output value at particular point x, $\star$ stands for convolution. This integral is defined as convolution of $f(x)$ and $g(x)$.

$$h(x) = f(x) \star g(x), \tag{2}$$

where, $g(x)$ is referred to as a blurring function or line spread function (LSF) or in two dimensions, the point spread function (PSF).

The Fourier transform of a convolution of two functions is the product of the Fourier transform of the two functions. Therefore, in the Fourier plane the effect becomes a multiplication, point by point, of the transform of $\widehat{F}(u)$ with the transfer function $\widehat{G}(u)$.

4. Atmospheric turbulence and speckle formation

Owing to the turbulent phenomena associated with heat flow and winds in the atmosphere, the density of air fluctuates in space and time. The inhomogeneities of the refractive index of the air can have devastating effect on the resolution achieved by any large telescope. The disturbance takes the form of distortion of the shape of the wavefront and variations of the intensity across the wavefront. Due to the motion and temperature fluctuations in the air above the telescope aperture, inhomogeneities in the refractive index develop. These inhomogeneities have the effect of breaking the aperture into cells with different values of refractive index that are moved by the wind across the telescope aperture.

Kolmogrov law represents the distribution of turbule sizes, from millimeters to meters, with lifetimes varying from milliseconds to seconds. Changes in the refractive index in different portions of the aperture result to the phase changes in the value of the aperture function. The time evolution of the aperture function implies that the point spread function is time dependent. When the Reynolds number exceeds some value in a pipe (depending on the geometry of the pipe), the transition from laminar flows to turbulent flows occur. The dimensionless quantity Reynolds number is defined as QL/ν, where Q is the mean flow speed, L is the transverse size of the pipe and ν is kinematic viscosity of the fluid. If L is taken as some characteristic size of the flow of atmosphere the result holds good for atmospheric case.

The power spectral density of refractive index fluctuations caused by the atmospheric turbulence follows a power law with large eddies having greater power (Tatarski, 1961). A plane wave propagating through the atmosphere of earth is distorted by refractive index variation in the atmosphere (troposphere); it suffers phase fluctuations and reaches the entrance pupil of a telescope with patches of random excursions in phase (Fried, 1966). Therefore, the image of the star in the focal plane of a large telescope is larger then the Airy disk of the telescope. The size is equivalent to the atmospheric point spread function (point spread function is a modulus square of the Fourier transform of the aperture function). The resolution at the image plane of the telescope is determined by the width of the PSF which is of the order of $(1.22\lambda/r_\circ)$, where, λ is a wavelength of light and $r_\circ$ is the average size of the turbulence cell, which is of the order of 10 cm. Therefore, resolution ($\sim$ 1 arc second) is unfortunately much larger then the theoretical size $1.22\lambda/D$ of the Airy disk of a large telescope (Rayleigh limit or diffraction limit), where, D is the diameter of the telescope.

The variance of phase difference fluctuations between any two points in the wave-front increases as the 5/3 power of their separation. When this variance exceeds π^2 rad for some separation $r_\circ$, then all details in the smaller than $\lambda/r_\circ$ will be obliterated in the long exposure images. If the exposure time is shorter than the evolution time of the phase inhomogeneities, then each patch of the wave-front with diameter $r_\circ$ − Fried parameter − would act independently of the rest of the wavefront resulting in multiple images of the source. These sub-images or 'speckles', as they are called and spread over the area defined by the long exposure image, can occur randomly along any direction within an angular patch of diameter $\lambda/r_\circ$. The average size of the speckle is of the same order of magnitude as the Airy disk of the telescope in the absence of atmospheric turbulence and the lifetime of individual speckle is of the order of 0.1 to 0.01 seconds. Figure 1 depicts the speckles of the star HR4689; observations were carried out at 2.34 meter VBT, Kavalur, India with the speckle interferometer (Saha et al., 1997, 1999a).

A snap shot taken later will show a different pattern but with similar probability of the angular distribution. A sum of similar exposures is the conventional image. It is easy to visualize that the sum of several statistically uncorrelated speckle patterns from a point source can result in an uniform patch of light a few arc-seconds wide (Saha, 1999b). figure 2 shows the result of summing 128 specklegrams demonstrating the destructions of finer details of the image by the atmospheric turbulence.

Venkatakrishnan et al., (1989) had also generated the intensity distribution for $r_\circ$ in the plane of a large telescope; the smallest contours have the size of

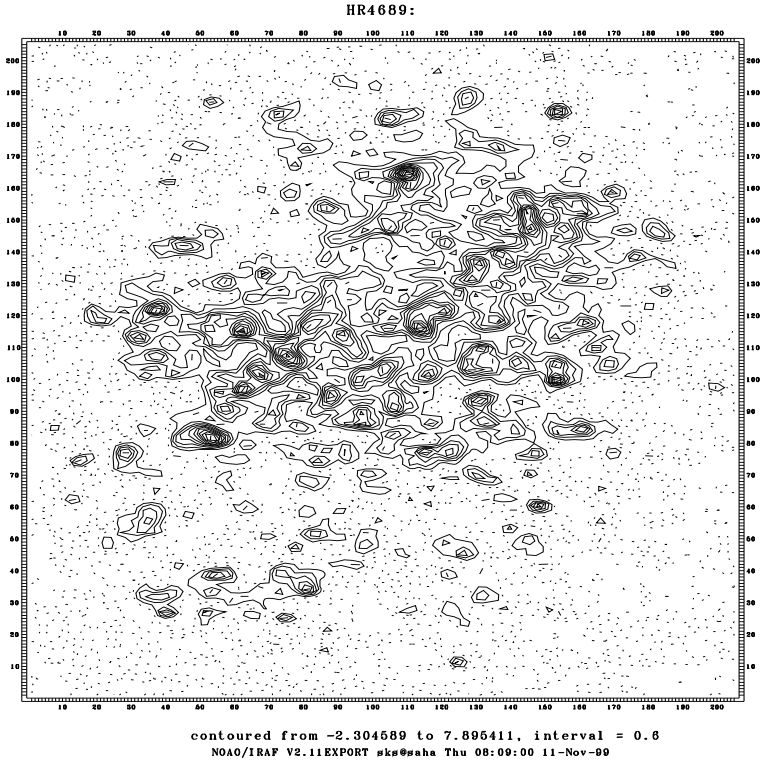

Figure 1: Specklegram of a binary star, HR4689 obtained at VBT, Kavalur, India.

the Airy disk of the telescope. The result of summing 100 such distributions showed similar concentric circle of equal intensity, destroying the finer details of an image. The method of such computer simulations runs as follows:

The intensity distribution in the focal point of the telescope for the atmospheric cell ($r_\circ$) of 10cm size and $L_\circ = 200$ cm for an entrance pupil of 200cm diameter were taken as samples. A power spectral density of the form

$$\rho(k) \propto \frac{L_\circ^{\frac{11}{3}}}{(1 + k^2 L_\circ^2)^{\frac{11}{6}}}, \tag{3}$$

was multiplied with a random phase factor $e^{i\phi}$, one for each value of (k_x, k_y), with ϕ uniformly distributed between $-\pi$ and π.

The resulting 2-D pattern in k_x, k_y space was Fourier transformed to obtain one realization of the wavefront $W(x, y)$. The Fraunhofer diffraction pattern of a

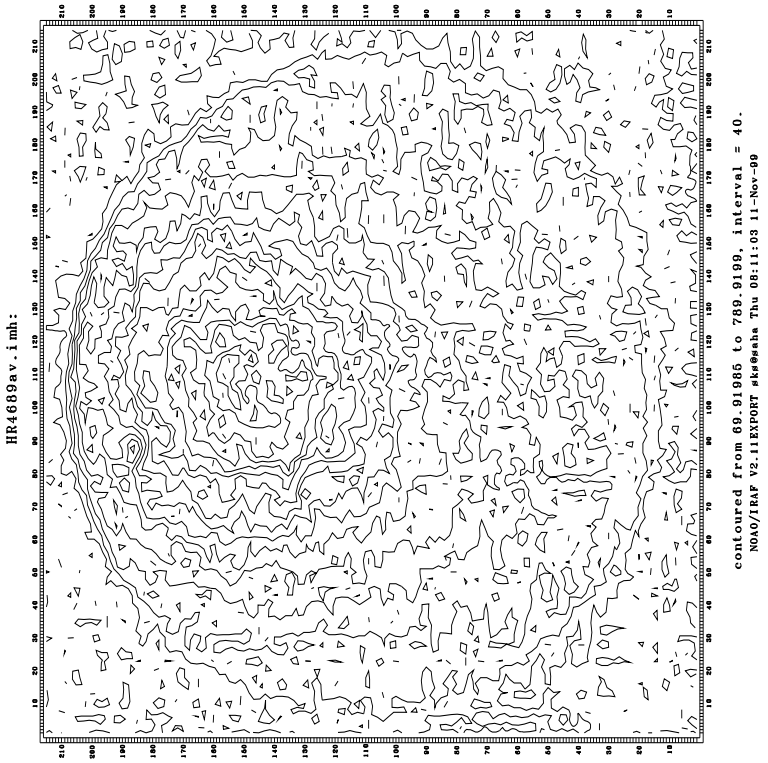

Figure 2: The result of summing 128 specklegrams of the same star, HR4689.

piece of this wavefront with the diameter of the entrance pupil gives angular distribution of amplitudes, while the squared modulus of this field gives the intensity distribution in the focal plane of the telescope.

The long-exposure PSF is defined by the ensemble average, $< S(x,y) >$, independent of any direction. The average illumination, $I(x,y)$ of a resolved object, $O(x,y)$ obeys convolution relationship,

$$< I(x,y) >= O(x,y) \star < S(x,y) >, \tag{4}$$

where, (x,y) is a 2-dimensional space vector. Using 2-dimensional Fourier transform, this equation can be read as,

$$< \widehat{I}(u,v) >= \widehat{O}(u,v) \cdot < \widehat{S}(u,v) >, \tag{5}$$

where, $\widehat{O}(u,v)$ is the object spectrum, $< \widehat{S}(u,v) >$ is the transfer function for long-exposure images and is the product of the transfer function of the atmosphere $\widehat{B}(u,v)$, as well as the transfer function of the telescope, $\widehat{T}(u,v)$.

(u, v) is the spatial frequency vector. The transfer function for long-exposure image can be expressed as,

$$< \widehat{S}(u,v) >= \widehat{B}(u,v) \cdot \widehat{T}(u,v). \tag{6}$$

The benefit of the short-exposure images over long-exposure can be visualized by the following explanation.

Let us consider two seeing cells separated by a vector in the telescope pupil, $\lambda(u, v)$, where λ is the mean wavelength. If a point source is imaged through the telescope by using pupil function consisting of two apertures, corresponding to the two seeing cells, then a fringe pattern is produced with narrow spatial frequency bandwidth. If the major component $\widehat{I}(u, v)$ at the frequency (u, v) is produced by contributions from all pairs of points with separations $\lambda(u, v)$, with one point in each aperture and is averaged over many frames, then the result for frequencies greater than r_o/λ tends to zero. The Fourier component performs a random walk in the complex plane and average to zero, $< \widehat{I}(u, v) > = 0$, when $u > r_o/\lambda$.

For a large telescope, the aperture, P, can be sub-divided into a set of sub-apertures, p_i. According to the diffraction theory (Born and Wolf, 1984) the image at the focal plane of the telescope is obtained by adding all such fringe patterns produced by all possible pairs of sub-apertures. With increasing distance of the baseline between two sub-apertures, the fringes move with an increasingly larger amplitude. On a long-exposure images, no such shift is observed, which implies the loss of high frequency components of the image. While, in the short-exposure images (<20 msec), the interference fringes are preserved.

4.1 Seeing

The common query for an observer is about 'seeing'. This important parameter changes very fast, every now and then. It is the total effect of distortion in the path of the light via different contributing layers of the atmosphere to the detector placed at the focus of the telescope (detail discussions can be found in recent article by Saha, 1999a). The major sources of image degradation predominantly comes from the surface layer, as well as from the aero-dynamical disturbances in the atmosphere surrounding the telescope and its enclosure, namely, (i) thermal distortion of primary and secondary mirrors when they get heated up, (ii) dissipation of heat by the latter mirror, (iii) rise in temperature at the primary cell, (iv) at the focal point causing temperature gradient close to the detector etc. Saha and Chinnappan (1999) have found that the seeing at VBT improved gradually in the latter part of the night.

The resolution θ of a large telescope, limited by the atmospheric turbulence, as defined by the Strehl criterion is

$$\theta = \frac{4}{\phi}\frac{\lambda}{r_o}, \tag{7}$$

Then the question arises how to measure seeing? The qualitative method is from the short exposure images using speckle interferometric technique, where, the area of the telescope aperture divided by the estimated number of speckles gives the wavefront coherence area σ, from which r_o can be found by using relation,

$$\sigma = 0.342\Big(\frac{r_o}{\lambda}\Big)^2. \tag{8}$$

If the autocorrelations of the short exposure images are summed, it contains autocorrelation of the seeing disk together with the autocorrelation of the mean speckle cell. It is width of the speckle component of the autocorrelation that provides information on the size of the object being observed (Saha and Chinnappan, 1999, Saha et al., 1999a).

Systematic studies of this parameter would enable to understand the various causes of the local seeing, for example, thermal inhomogeneities associated with the building, aberrations in the design, manufacture and alignment of the optical train etc.

Doom seeing plays a vital role in deteriorating image quality. It is necessary to take precautionary measure to avoid hot air entrapment. The important ones are (i) bring down the control room from the observing floor, (ii) improve the cross ventilation at each of the floors, (iii) remove unused machines or any other equipments, excess cemented portions available around the building, as well as all glass enclosures from the building.

Mirror seeing is another important source of image spread and has the longest time-constant. The spread amounts to 0.5" for a 1° different in temperature. Therefore, It is essential to make arrangement to cool the primary mirror and try to maintain uniform temperature in and around the primary mirror cell (Saha and Chinnappan, 1999).

5. Speckle

The term 'Speckle' refers to a grainy structure observed when an uneven surface of an object is illuminated by a fairly coherent source. A good example of speckle phenomena may be observed at the river port when many boats are approaching towards the former at a particular time or in the swimming pool when many swimmers are present. Each boat or swimmer emits wave trains and interference between these random trains causes a speckled wave field on the water surface. Depending on the randomness of the source, spatial or temporal, speckles tend to appear. Spatial speckles may be observed when all parts of

the source vibrate at same constant frequency but with different amplitude and phase, while temporal speckles are produced if all parts of it have uniform amplitude and phase. With a non-monochromatic vibration spectrum, in the case of random sources of light, spatio-temporal speckles are produced.

The ground illumination produced by any star has fluctuating speckles, known as star speckles. It is too fast and faint, therefore, cannot be seen directly. Atmospheric speckles can be observed easily in a star image at the focus of a large telescope using a strong eyepiece. The star image looks like a pan of boiling water. If a short exposure image is taken, speckles can be recorded. The number of correlation cells is determined by the equation $N = D/r_o$. As the seeing improves, the number decreases. It is clear that speckles are caused by interference effect between wave element having random phases, rather then by ray bending effect. Its structure in astronomical images is the result of constructive and destructive bi-dimensional interferences between rays coming from different zones of incident wave. The statistical properties of speckle pattern depend both on the coherence of the incident light and the properties of random medium.

Mathematically, speckles are simply the result of adding many sine functions having different, random characteristics. Since the positive and negative values cannot cancel out everywhere, adding an infinite number of such sine functions would result in a function with 100% constructed oscillations.

5.1 Imaging in the Presence of Atmosphere

In the ideal condition, the resolution can be achieved in an imaging experiment, is limited only on imperfections in the optical system. If a collimated beam passes through the atmosphere and is collected by a telescope, the quality of the image formed is influenced by the atmospherically produced disturbances.

Let the modulation transfer function (MTF) of an optical system be composed of the atmosphere and a telescope. The random wavefront tilt displaces the image but does not reduce its sharpness. If a short exposure is recorded, the image sharpness and MTF are insensitive to the tilt. While, in the case of long exposure ($>$ 20 msec) image, the image is spread during the exposure by its random variations of the tilt. Therefore, the image sharpness and the MTF are affected by wavefront tilt, as well as by the more complex shapes. In the short exposure case, a random factor associated with the tilt is extracted from the MTF before being taken the average, where in the long exposure case, no such factor is removed.

Let us consider an imaging system consists of a simple lens based telescope in which the point spread function (PSF) is invariant to spatial shifts. An object (point source) at a point (x', y') anywhere in the field of view will, therefore, produce a pattern $S[(x, y) - (x', y')]$ across the image. If the object can emit

incoherently, the image $I(x, y)$ of a resolved object $O(x, y)$ obeys a convolution relationships. The mathematical description of the convolution of two functions is of the form:

$$I(x, y) = \int O(x', y')S[(x, y) - (x', y')]d(x', y'), \tag{9}$$

5.2. Outline of the theory of speckle interferometry

By integrating autocorrelation function of the successive short-exposure records rather than adding the images themselves, the diffraction-limited information can be obtained. Indeed, autocorrelation function of a speckle images preserves some of the information in the way which is not degraded by the co-adding procedure. For each of the short-exposure instantaneous record, the quasi-monochromatic incoherent imaging equation applies,

$$I(x, y) = O(x, y) \star S(x, y), \tag{10}$$

where, $I(x, y)$ is the instantaneous image intensity, $O(x, y)$ the object intensity, $S(x, y)$ the instantaneous PSF.

The analysis of data may be carried out in two equivalent ways. In the spatial domain the ensemble average space autocorrelation is found giving the resultant imaging equation.

In the Fourier plane the effect becomes a multiplication, point by point, of the transform of the object $\widehat{O}(u, v)$ with the transfer function $\widehat{S}(u, v)$, and therefore, equation 10 leads to,

$$\widehat{I}(u, v) = \widehat{O}(u, v) \cdot \widehat{S}(u, v). \tag{11}$$

The ensemble average of the power spectrum is given by,

$$< |\widehat{I}(u, v)|^2 >= |\widehat{O}(u, v)|^2 \cdot < |\widehat{S}(u, v)|^2 > . \tag{12}$$

Hence, if $< |\widehat{S}(u, v)|^2 >$ is known, $|\widehat{O}(u, v)|^2$ can be estimated. To find this, one has to observe a point source close to the object. The Fourier transform of a point source (delta function) is a constant, C_n. Then, equation 12, for a point source is

$$< |\widehat{I}_s(u, v)|^2 >= C_n^2 \cdot < |\widehat{S}(u, v)|^2 > . \tag{13}$$

To find ${C_n}^2$, one has to find the boundary condition. At the origin of the Fourier plane, $S(u = 0, v = 0)$ is unity. This is true for an incoherent source. Hence, ${C_n}^2$ is given by,

$$C_n^2 = < |\widehat{I}_s(0,0)|^2 > / < |\widehat{S}(0,0)|^2 \ >, \tag{14}$$

i.e.,

$$C_n^2 = < |\widehat{I}_s(0,0)|^2 \ > . \tag{15}$$

Using equation 15 in equation 13 gives,

$$< |\widehat{S}(u,v)|^2 \ >= < |\widehat{I}_s(u,v)|^2 \ > / \ < |\widehat{I}_s(0,0)|^2 \ > . \tag{16}$$

From equations 16 and 11, the power spectrum of the object is given by

$$|\widehat{O}(u,v)|^2 = < |\widehat{I}(u,v)|^2 \ > /[< |\widehat{I}_s(u,v)|^2 \ > / \ < |\widehat{I}_s(0,0)|^2 \ ], \tag{17}$$

i.e., the power spectrum of the object is the ratio of the average power spectrum of the image to the normalized average power spectrum of the point source. By Wiener-Kinchin theorem, the inverse Fourier transform of equation 17 gives the autocorrelation of the object.

$$A[O(x,y)] = FT^{-}[|\widehat{O}(u,v)|^2], \tag{18}$$

where, A stands for autocorrelation.

6. Observational technique at VBT

The programme of observing close binary systems (separation $< 1''$) has been going on since 1996 using speckle interferometer at the Cassegrain focus of the 2.34 VBT, Kavalur, India (Saha, 1999a). The details of this interferometer can be found in the articles (Saha et al., 1997, 1999a), that samples the image scale at the Cassegrain focus of the said telescope to 0.015" per pixel of the intensified CCD. The wave-front falls on the focal plane and passes on to a microscope objective through a circular aperture of $\sim$350 μm of an optical flat kept at an angle of 15°. This aperture was developed on a low expansion optical glass by devising a fine grinding precision mechanism at the laboratory (A. P. Jayarajan and S. K. Saha). The aperture was ground into the glass held at the angle of 75° with respect to the grinding axis. Interested readers may try it out to repeat the same.

The enlarged beam is recorded after passing through a narrow band filter by a Peltier-cooled ICCD (386×576) camera as detector which offers various option of exposure time, viz., 1 msecs, 5 msecs, 10 msecs, 20 msecs etc. It can operate in full frame, frame transfer and kinetic modes. Since CCD is cooled to $\sim$40°, the dark noise is considerably low. Unlike the uncooled ICCD where data is stored in 8 bits, in this system, data is stored to 12 bits and can be archived to a Pentium PC. In full frame, as well as in frame transfer modes, the region of

interests can be acquired at a faster speed. While in the kinetic mode, the image area can be kept small to satisfy requirements, therefore, the rest of the area is usable for the data storage. The surrounding star field of diameter $\sim \phi$ 10 mm gets reflected from the optical flat on to a plane mirror and is re-imaged on to an uncooled ICCD (Chinnappan et al., 1991) for guiding the object.

7. Summary

Among others the most important observations made by means of speckle interferometry is the discovery of compact cluster, R136a (HD38268), of Doradus nebula in the Large Magallanic Clouds (Weigelt and Baier, 1985). Recent observations with adaptive optics system (Brandl et al., 1996) have revealed over 500 stars within the field of view 12.8"×12.8" covering a magnitude range 11.2. Baba et al., (1994) have observed a binary star, ϕ *And* (separation 0.53") using imaging speckle spectroscopic method and found that the primary star (Be star) has an Hα emission line while the companion has an Hα absorption line.

Developments of high angular resolution imaging have been going on in our Institute over a decade. Several experiments have been conducted at Vainu Bappu Observatory (Saha et al., 1987). The programme of speckle imaging at VBT has been a successful one. Now we are in a position to obtain informations of Fourier phase of the objects too (Saha et al., 1999b). Mapping of the certain interesting objects, viz., active galactic nuclei, proto-planetary nebulae will be undertaken in near future.

References

Anderson J. A., 1920, Astrophys. J., **51**, 263.
Baba N., Kuwamura S., Miura N., Norimoto Y., 1994, Ap. J., **431**, L111.
Born M., Wolf E., 1984, Principles of Optics, Pergamon Press.
Brandl B., Sams B. J., Bertoldi F., Eckart A., Genzel R., Drapatz S., Hofmann R., Lowe M., Quirrenbach A., 1996, Ap. J., **466**, 254.
Brown R. H., 1974, 'The Intensity Interferometry, its Applications to Astronomy', Taylor & Francis, London.
Brown R. H. and Twiss R. Q., 1958, Proc. Roy. Soc. A., **248**, 222.
Brown R. H., Davis J. and Allen L. R., 1967, MNRAS, **137**, 375.
Brown R. H., Jennison R. C. and Das Gupta M. K., 1952, Nature, **170**, 1061.
Chinnappan V., Saha S. K., Faseehana, 1991, Kod. Obs. Bull. **11**, 87.
Fizeau H., 1868, C. R. Acad. Sci. Paris, **66**, 934.
Fried D. C., 1966, J. Opt. Soc. Am., **56**, 1972.
Goodman J. W., 1968, Introduction to Fourier optics, McGraw Hill Book Co. NY.

Labeyrie A., 1970, Astron. & Astrophys., **6**, 85.
Labeyrie A., 1975, Astrophys. J., **196**, L71.
Labeyrie A., 1985, 15th. Advanced Course, Swiss Society of Astrophys. and Astron. ed.. A. Benz, M. Huber and M. Mayor, 170.
Labeyrie A., Schumacher G., Dugué M., Thom C., Bourlon P., Foy F., Bonneau D. and Foy R., 1986, Astron. & Astrophys., **162**, 359.
Michelson A. A., 1920, Astrophys. J., **51**, 257.
Michelson A. A., and Pease F. G., 1921, Astrophys. J., **53**, 249.
Mourard D., Bosc I., Labeyrie A., Koechlin A. and Saha S., 1989, Nature, **342**, 520.
Saha S. K., 1999a, Bull. Astron. Soc. Ind., **27**, 443.
Saha S. K., 1999b, Ind. J. Phys., **73b**, 553.
Saha S. K., Chinnappan V., 1999, Bull. Astron. Soc. Ind., **27**, 327.
Saha S. K., Jayarajan A. P., Sudheendra G., Umesh Chandra A., 1997, Bull. Astron. Soc. Ind., **25**, 379.
Saha S. K., Sridharan R., Sankarasubramanian K., 1999b, submitted to Bull. Astron. Soc. Ind.
Saha S. K., Sudheendra G., Umesh Chandra A., Chinnappan V., 1999a, Exp. Astron, **9**, 39.
Saha S. K., Venkatakrishnan P., Jayarajan A. P., Jayavel N., 1987, Curr. Sci., **56**, 985.
Tatarski V. I., 1961, 'Wave Propagation in a Turbulent Medium' McGraw Hill.
Venkatakrishnan P., Saha S. K., Shevgaonkar R. K., 1989, Proc. 'Image Processing in Astronomy', ed., T. Velusamy, 57.
Weigelt G., Baier G., 1985, A & A., **150**, L18.

Appendix I

Theorems of Fourier Transform

1. Linearity theorem

$$F(\alpha g + \beta h) = \alpha F(g) + \beta F(h) \tag{19}$$

i.e., the transform of sum of two functions is simply the sum of their individual transforms.

2. Similarity theorem

A stretching of the co-ordinates in the space domain (x, y) results in the construction of the co-ordinates in the frequency domain $(f_x,\ f_y)$ plus a change in the overall amplitude of the spectrum. i.e., if

$$F(g(x, y)) = G(f_x, f_y) \tag{20}$$

then,

$$F(g(ax + by)) = G(f_x/a, f_y/b)/|ab| \tag{21}$$

3. Shift theorem

Translation of a function in a space domain introduces a linear phase shift in the frequency domain. i.e., if

$$F(g(x, y)) = G(f_x, f_y) \tag{22}$$

then,

$$F(g(x - a, y - b)) = G(f_x, f_y) \exp(-2\pi j(f_x a + f_y b)) \tag{23}$$

4. Perseval's theorem

This theorem is generally interpretable as a statement of conservation of energy. It says that the total energy in the real domain is equal to the total energy in the Fourier domain. i.e.,

$$F(g(x, y)) = G(f_x, f_y) \tag{24}$$

then

$$\int_{-\infty}^{+\infty} \int_{-\infty}^{+\infty} |g(x, y)|^2 dxdy = \int_{-\infty}^{\infty} \int_{-\infty}^{\infty} |G(f_x, f_y)|^2 df_x df_y \tag{25}$$

5. Convolution Theorem

The convolution of two functions in the space domain (an operation that will be found to arise frequently in the theory of linear system) is entirely equivalent of the more simple operation of multiplying their individual transform. i.e.,

$$F(g(x, y)) = G(f_x, f_y) \tag{26}$$

and

$$F(h(x,y)) = H(f_x, f_y) \tag{27}$$

then

$$F(\int_{-\infty}^{+\infty}\int_{-\infty}^{+\infty} g(\xi,\eta)h(x-\xi,y-\eta)d\xi d\eta) = G(f_x,f_y)H(f_x,f_y) \tag{28}$$

6. Autocorrelation theorem

This theorem may be regarded as special case of convolution theorem. The Fourier transform of autocorrelation of a function is the squared modulus of the Fourier transform. i.e. if

$$F(g(x,y)) = G(f_x, f_y) \tag{29}$$

then,

$$F(\int_{-\infty}^{+\infty}\int_{-\infty}^{+\infty} g(\xi,\eta)g^*(\xi-x,\eta-y)d\xi d\eta) = |G(f_x,f_y)|^2 \tag{30}$$